arXiv:1610.09399v1 [cond-mat.str-el] 28 Oct 2016

Optical and spin-Hall conductivities of Rashba conducting strips coupled to ferro- and antiferromagnetic layers

José A. Riera
Instituto de Física Rosario (CONICET) and Universidad Nacional de Rosario, Rosario, Argentina
(Dated: November 1, 2016)

A system composed of a conducting planar strip with Rashba spin-orbit coupling (RSOC), magnetically coupled to a layer of localized magnetic moments, at equilibrium, is studied within a microscopic Hamiltonian with numerical techniques at zero temperature. In particular, transport properties for the cases of ferromagnetic (FM) and antiferromagnetic (AFM) coupled layers are computed in linear response on strips of varying width. The case of uncoupled Rashba strips is also studied for comparison. In the case of Rashba strips coupled to an AFM localized order, results for the optical conductivity, for small strip widths, suggest the proximity to a metal-insulator transition. More interesting, in the proximity of this transition, and in general at intermediate values of the RSOC, it is observed a large spin-Hall conductivity that is two orders of magnitude larger than the one for the FM order for the same values of the RSOC and strip widhts. There are clearly two different regimes for small and for large RSOC, which is also present in the behavior of Rashba helical currents. Different contributions to the optical and the spin-Hall conductivities, of inter- or intraband origin, or coming from the hopping or spin-orbit terms of the Hamiltonian, are examined. Finally, the stability of the AFM order when magnetic moments are allowed to rotate is studied.

I. INTRODUCTION

There is currently an increasing interest in studying and developing new systems and devices that could process information using the spin of the electron, which is the essence of the field of spintronics.[1–4] In particular, a considerable number of possibilities stem from the implementation of effective couplings derived from microscopic spin-orbit (SO) interactions, chief among them the Rashba spin-orbit coupling (RSOC) which appears in systems with structural inversion asymmetry.[5–8]

It has been recently noticed[9–12] that a strong spin torque can be induced on ferromagnets (FM) coupled to a two-dimensional (2D) layer with Rashba SOC. This process was observed when an electrical current flows in the plane of a Co layer with asymmetric Pt and AlOx interfaces.[12,13] Even more recently, it has been discussed the possibility of an analogous relativistic SO torque appearing when an antiferromagnetic (AFM) layer is coupled to a conducting layer containing RSOC.[14,15] It was also suggested that this possibility could be realized in bulk Mn_2Au, which although is centrosymmetric, it can be divided into two sublattices that separately have broken inversion symmetry. This second possibility is referred to as a Néel SO torque (NSOT), to differentiate it from the previously mentioned FM SO torque (FSOT). In these two systems, the FM or AFM order in the magnetic layer is fixed due to a large enough exchange interaction among localized magnetic moments. Possible advantages of spintronic devices involving AFM layers, for example their fast magnetic dynamics and the insensitivity to stray fields, are well-known.[16,17] Remarkably, it was recently found that the NSOT could drive an antiferromagnetic domain wall at velocities two orders of magnitude greater than the ones in ferromagnets.[18,19]

Rashba SO coupling leads to the spin-Hall effect[7,8] which manifests itself on finite width systems or strips, as spin accumulation at the strip edges.[20–22] Perhaps the most important quantity related to these effects is the spin-Hall conductivity which in clean 2D systems turned out to be a constant independent of the Rashba strength for a wide range of electron fillings.[23] Subsequent studies lead to the conclusion that the spin-Hall conductivity vanishes in the presence of scattering.[24] This result led in turn to some controversial interpretation of experimental data. Most of this theoretical work has been performed on unbounded 2D systems and using a parabolic band, that is, with infinite bandwidth. Many shortcomings and peculiar results obtained for these systems have been stressed in the literature. Specifically, the above mentioned controversy concerning the spin-Hal conductivity was settled down once the effect of parabolic bands was recognized.[25] On the other hand, planar strips, rather than unbounded 2D systems, and tight-binding bands with finite bandwidth, are in general more realistic, particularly for new materials or mechanisms which have been proposed for spintronic devices and where larger electron fillings may be involved, such as for example, those involving $LaAlO_3/SrTiO_3$ interfaces.[26,27]

Hence, the purpose of the present work is to study the optical and spin-Hall conductivities of conducting strips with a Rashba SOC in contact with a magnetized slab with FM or AFM orders. Although the above mentioned FSOT and NSOT occur in off-equilibrium systems, the study of an appropriate microscopic model Hamiltonian in second quantization at equilibrium, and within linear response, could shed some light on the behavior of systems in off-equilibrium regimes, particularly for strips. For the sake of comparison, the case of isolated Rashba conducting strips, that is, not connected to a magnetic layer, will also be studied. At equilibrium, it is also interesting to examine the Rashba helical currents,[28] which appear due to the presence of open boundaries, and it will be shown that their behavior is correlated with the

one observed through the optical and spin-Hall conductivities. These studies are performed assuming that the magnetic moments are always collinear. Although this assumption is realistic since the exchange interaction between moments in the coupled layer is typically very large,[19] in the final Section various possible instabilities of the AFM order obtained by minimizing the Hamiltonian with respect to arbitrary orientation of the magnetic moments will be examined.

II. MODEL AND METHODS

The Hamiltonian here studied is $H = H_0 + H_{int}$ where[15,29]:

$$H_0 = -t \sum_{<l,m>,\sigma} (c^\dagger_{l\sigma} c_{m\sigma} + H.c.) + \lambda \sum_l [c^\dagger_{l+x\downarrow} c_{l\uparrow} - c^\dagger_{l+x\uparrow} c_{l\downarrow} + i(c^\dagger_{l+y\downarrow} c_{l\uparrow} + c^\dagger_{l+y\uparrow} c_{l\downarrow}) + H.c.]$$
$$H_{int} = -J_{sd} \sum_l \mathbf{S}_l \cdot \hat{\mathbf{s}}_l + J \sum_{<l,m>} \mathbf{S}_l \cdot \mathbf{S}_m \quad (1)$$

where l, m are sites on a square lattice, located on the $\{x, y\}$-plane, $\mathbf{S}_l$ are the localized magnetic moments, assumed classical, and $\hat{\mathbf{s}}_l$ are the spin of the conduction electrons (its operator nature is made explicit for later usage). The longitudinal (transversal) direction of the strip corresponds to the x axis (y axis). H_0 is the non-interacting part, which includes the hopping and RSOC terms with coupling constants t and λ, respectively. The RSOC term corresponds to an effective Rashba electric field along the z-axis, i.e. perpendicular to the plane of the strip. Since both terms in H_0 contribute to the total kinetic energy, we choose the normalization $t^2 + \lambda^2 = 1$, whose square root will then be adopted as the unit of energy. With this normalization, the kinetic energy, and hence the total energy for fixed J, J_{sd}, turns out to be approximately constant as λ/t is varied.[29] Hence, all the physical properties studied in the following will solely depend on the ratio λ/t, for given values of J, J_{sd}. The interacting part of the Hamiltonian contains a ferromagnetic coupling between conduction electrons and localized magnetic moments with strength J_{sd}, and an exchange interaction between magnetic moments with coupling J. Hamiltonian (1) is just a ferromagnetic Kondo lattice model with a Rashba SO coupling.

For the FM case, a value of $J_{sd} = 10$ will be adopted, which corresponds to the case of well-separated spin-up and spin-down conduction bands. For $J_{sd} = 5$, the bands are partially separated and in this case the AFM would be energetically favourable if they are allowed to rotate, for $J = 0$.[30] For this reason the AFM order will be studied for $J_{sd} = 5$, although some results for $J_{sd} = 10$ will be also presented. In general, results do not qualitative change in this range of J_{sd}. Since FM and AFM orders are put by hand, the value of J is irrelevant since it only adds a constant to the total energy. The direction of the magnetic moments is adopted to be along the z-axis. Since model (1) corresponds to a quantization axis along the z-axis, it is expected that results will depend on the direction of the magnetic moments, and this issue will be examined in the final section. In addition, for small values of $|J|$, even in equilibrium, if the individual magnetic moments are allowed to freely rotate, both the FM and the AFM states will become unstable with respect to various spiral and double spiral states. The study of some of these instabilities is also deferred to the final section.

Hamiltonian (1) will be studied on strips of length L and width W, with periodic (open) boundary conditions along the longitudinal (transversal) direction. $N = LW$, is the number of sites on the strip.

For classical localized magnetic moments, which is the assumption usually adopted in this context, the Hamiltonian becomes an extended tight-binding problem which is solved by numerical exact diagonalization for clusters with $2 \leq W \leq 64$ and $256 \leq L \leq 8000$. In all results presented below, finite size effects with respect to L are negligible. All results presented below correspond to quarter filling, $n = 0.5$.

The main quantities studied are the spin-conserving currents, $J_{\sigma,\hat{\mu}}$, $\sigma = \uparrow, \downarrow$, $\hat{\mu} = x, y$, defined as the expectation value of the operator:

$$\hat{j}_{\sigma,l,\hat{\mu}} = it(c^\dagger_{l+\hat{\mu},\sigma} c_{l,\sigma} - H.c.), \quad (2)$$

in units where the electron charge $e = 1$, and $\hbar = 1$, and the spin-flipping currents, $J_{SO,\hat{\mu}}$, which are the expectation value of the operators:

$$\hat{j}_{SO,l,\hat{x}} = -i\lambda(c^\dagger_{l+x\downarrow} c_{l\uparrow} - c^\dagger_{l+x\uparrow} c_{l\downarrow} - H.c.)$$
$$\hat{j}_{SO,l,\hat{y}} = \lambda(c^\dagger_{l+y\downarrow} c_{l\uparrow} + c^\dagger_{l+y\uparrow} c_{l\downarrow} + H.c.) \quad (3)$$

These expressions can be obtained in an standard way by introducing appropriate Peierls factors in the Hamiltonian (1) and taking the first derivative with respect to the magnetic flux. These currents also satisfy the charge conservation law, given generically by $\hat{j} = -\partial n/\partial\tau$, where n is the occupation number operator and τ is the time, as long as $\partial n/\partial\tau = i[H_0, n]$, which will be further discussed below.

In equilibrium, due to translation invariance along x, all currents along x depend only on the chain position given by y. In all the cases analyzed below, in the absence of external electromagnetic sources, the SO currents along the strip direction are zero, and all vertical currents are also zero, except for the case of a constant orientation of the magnetic moments forming an angle $\theta = \pi/3$ considered in Section V, where a more complex pattern appears.

III. RASHBA HELICAL CURRENTS

The Rashba helical currents (RHCs), are counter-propagating spin-up and spin-down electron currents, that is of hopping or spin-conserving nature, at each link

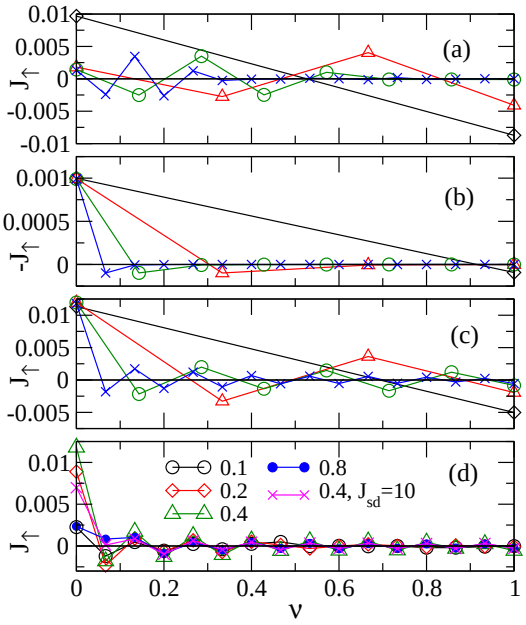

FIG. 1. (Color online) Spin-up current on each chain as a function of the depth of the chain ($\nu = 0$, edge, $\nu = 1$, center chain), for $\lambda/t = 0.4$, (a) isolated Rashba conducting strip ($J_{sd} = 0$), (b) FM layer, $J_{sd} = 10$, and (c) AFM layer, $J_{sd} = 5$. Results correspond to strips with width $W = 4$ (diamonds), 8 (up triangles), 16 (circles), and 32 (crosses). In (d), Spin-up currents are shown for various values of λ/t indicated on the plot, AFM layer, $J_{sd} = 5$ (except the one corresponding to $J_{sd} = 10$), $W = 32$.

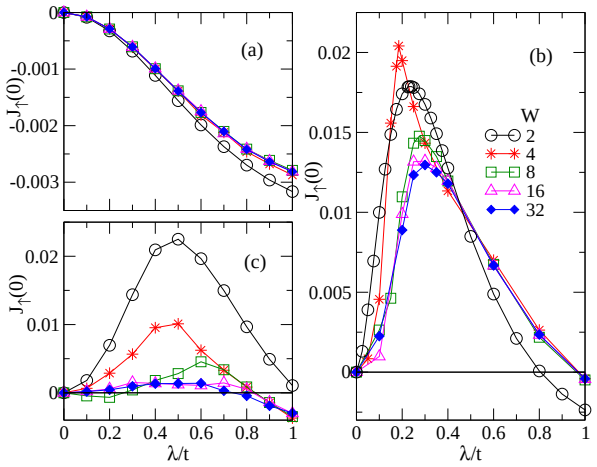

FIG. 2. (Color online) Spin-up current on the edge chain as a function of λ/t, for various strip width W indicated on the plot, (a) fixed FM state $J_{sd} = 10$, (b) fixed AFM state $J_{sd} = 5$, and (c) isolated Rashba strip, $J_{sd} = 0$.

at the lattice,[28] and they appear due to the RSOC acting on both x and y directions on the strip, in equilibrium and in the absence of any external electromagnetic field. It should be emphasized that they appear as a consequence of some boundary imposed on the system, or eventually in the presence of impurities.[31] Their existence can be inferred at an effective level[28] or by the structure of the RSOC.[31,32] Of course, the total current along the strip is zero. In the following we will compute RHCs, defined by the spin-up current along x, $J_\uparrow$, on each chain of closed strips of width W.

The RHCs on each chain as a function of its distance ν to the edge ($\nu = 0$, edge chain ($y = W$), $\nu = 1$, center chain ($y = W/2 + 1$)) are shown in Fig. 1(a-c) for various strip widths, $\lambda/t = 0.4$, and different orderings of the magnetic layer. Fig. 1(a) corresponds to conducting strips decoupled from the magnetic layer, that is $J_{sd} = 0$. This is the case previously studied, presenting characteristic sign oscillations with wavevector π, at $n = 0.5$, and mostly concentrated near the edges.[28] In Fig. 1(b), the conducting strip is coupled to a FM layer by a large value of $J_{sd} = 10$, corresponding to well-separated $s^z > 0$ and $s^z < 0$ bands, where $s^z =< \hat{s}^z >_{sp}$, $< ... >_{sp}$ meaning the average over a single-particle state. This is not a fully polarized system in the sense that for each band, $|s^z| < 1/2$. In this case, RHCs are only noticeable from zero at the strip edge, and effects of finite strip width are negligible. Sign oscillations are mostly absent. A very different behavior is observed for the case of an AFM spin background, as shown in Fig. 1(c). In this case, RHCs are also maximal near the edge. At the edge, $J_\uparrow(\nu = 0)$ is more than an order of magnitude larger than the one for the FM case, and it does not depend on the strip width. Besides, similarly to the decoupled system, they present sign oscillations as a function of ν. Notice also that the direction of $J_\uparrow(\nu = 0)$ is the same as the one for the pure Rashba strip and is opposite to the one of the FM coupled layer case.

The dependence of RHCs with λ/t for the AFM background, for $W = 32$ and $J_{sd} = 5$, is shown in Fig. 1(d). It is apparent that $J_\uparrow(\nu)$ grows with λ/t up to $\lambda/t \approx 0.4$, in the same way that it was predicted and observed for the case of isolated conducting strips,[28] and then it starts to decrease for larger λ/t. By increasing J_{sd}, the RHCs decreases, as is illustrated for $\lambda/t = 0.4$ and $J_{sd} = 10$.

For a more systematic study, from now on only the RHCs on the outermost chains will be considered. In Fig. 2 the values of the RHC on the edge chain ($\nu = 0$) of strips with various widths are shown for different magnetic coupled layers as a function of λ/t. It can be seen in Fig. 2(a) that for the FM layer, the edge RHC in absolute value increases monotonically with λ/t in the range considered, with an initial shape which approximately follows the predicted quadratic dependence for systems in the presence of a boundary.[28] At $\lambda/t \approx 0.5$, $J_\uparrow(0)$ experiences a change of curvature. This behavior is also virtually independent of W except for the smallest width considered, $W = 2$. In contrast, RHCs on the edge chains follow a non-monotonic behavior for the AFM layer, as shown in Fig. 2(b). In this case, $J_\uparrow(0)$ presents a strong peak located at $0.2 \leq (\lambda/t)_{peak} \leq 0.3$ for all W. The dependence with W is nonmonotonic for $\lambda/t \leq (\lambda/t)_{peak}$, with the largest peak reached for $W = 4$. This peak be-

comes smoother and shifts to larger values of λ/t as W increases, although this variation with W seems to have converged for $W \approx 32$. It can be observed also that the the RHC curves in the region of $\lambda/t > (\lambda/t)_{peak}$, fall onto a single curve, that is, they become independent of the strip width. Eventually $J_\uparrow(0)$ decreases to zero for $\lambda/t \approx 1$ for all W. Remarkably, for λ/t closer to the peak position, the RHCs for the AFM coupled layer are one order of magnitude larger than for the FM layer for all W, in agreement with the results shown in Fig. 1(b,c).

Results for the isolated conducting Rashba strip, $J_{sd} = 0$, are shown in Fig. 2(c) for comparison. $J_\uparrow(0)$ presents a broad maximum for $\lambda/t \approx 0.5$, that is larger than the peak of the AFM coupled layer for $W = 2$ but decreases rapidly by increasing W. Again the dependence with W seems to be converged for $W \approx 32$.

IV. TRANSPORT PROPERTIES

In this section, the main transport properties appearing as the response to some applied electromagnetic field, and that determine the suitability of Rahsba strips coupled to magnetic layers for spintronic applications, that is, the optical conductivity and the spin-Hall conductivity, are going to be studied. It is also important to examine if the behavior of the Rashba helical currents observed in the preceding section can be correlated with the behavior of these transport properties.

The optical conductivity is defined as the real part of the linear response to an electric field and can be written as:[33]

$$\sigma(\omega) = D\delta(\omega) + \sigma^{reg}(\omega) \tag{4}$$
$$= D\delta(\omega) + \frac{\pi}{N}\sum_{n\neq 0}\frac{|\langle\Psi_n|\hat{j}_x|\Psi_0\rangle|^2}{E_n - E_0}\delta(\omega - (E_n - E_0))$$

where the paramagnetic current along the x-direction is defined in terms of the currents defined in Eqs. (2,3) as:

$$\begin{aligned}\hat{j}_x &= \hat{j}_{hop,x} + \hat{j}_{SO,x}\\ \hat{j}_{hop,x} &= \hat{j}_{\uparrow,x} + \hat{j}_{\downarrow,x}\\ \hat{j}_{\sigma,x} &= \sum_l \hat{j}_{\sigma,l,x}, \quad \sigma = \uparrow,\downarrow\\ \hat{j}_{SO,x} &= \sum_l \hat{j}_{SO,l,x}\end{aligned} \tag{5}$$

The Drude weight D is calculated from the f-sum rule as:

$$\frac{D}{2\pi} = -\frac{\langle H_{0,x}\rangle}{2N} - I_{reg} \tag{6}$$

where $-\langle H_{0,x}\rangle$ is the total kinetic energy of electrons along the x-direction, and

$$I_{reg} = \frac{1}{N}\sum_{n\neq 0}\frac{|\langle\Psi_n|\hat{j}_x|\Psi_0\rangle|^2}{E_n - E_0} \tag{7}$$

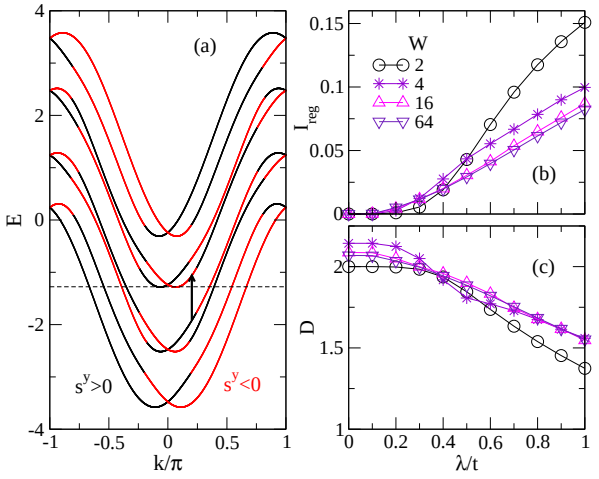

FIG. 3. (Color online) (a) Energy bands with $s^y > 0$ (black) or $s^y < 0$ (red), $W = 4$, $\lambda/t = 0.4$. k is the momentum along the longitudinal direction. The dashed line indicates the chemical potential. (b) Integral of the regular part of the optical conductivity, and (c) Drude weight, as a function of λ/t for various strip widths W. Isolated, $J_{sd} = 0$, $L = 2000$ Rashba strips.

Notice that from Eq. (1), $\langle H_{0,x}\rangle = \langle H_{0,hop,x}\rangle + \langle H_{0,SO,x}\rangle$. In addition, taking into account the two contributions to the total current, given by Eq. (5), I_{reg} has a contribution from hopping currents, $|\langle\Psi_n|\hat{j}_{hop,x}|\Psi_0\rangle|^2$, another contribution from SO currents, $|\langle\Psi_n|\hat{j}_{SO,x}|\Psi_0\rangle|^2$, and the contribution from the cross terms, $2Re\{\langle\Psi_n|\hat{j}_{hop,x}|\Psi_0\rangle\langle\Psi_0|\hat{j}_{SO,x}|\Psi_n\rangle\}$.

The spin-Hall conductivity σ_{sH} is defined as the $\omega = 0$ limit of the spin-charge transversal response function given by the Kubo formula, at zero temperature:[23,24]

$$\sigma^{sc}_{xy}(\omega) = -i\frac{1}{\pi N}\sum_n\sum_m \frac{\langle\Psi_n|\hat{j}^s_y|\Psi_m\rangle\langle\Psi_m|\hat{j}_x|\Psi_n\rangle}{[(E_n - E_m)^2 - \omega^2]} \tag{8}$$

where j^s_y is the spin current along the y-direction. In the first sum, the summation is performed only over states with energies E_n larger than the Fermi energy E_F, and in the second sum only over states with energies $E_m < E_F$. The spin current along the transversal direction is defined as:[23,24]

$$\hat{j}^s_{y,l} = \frac{\partial\hat{s}^z_l}{\partial\tau} = i[H_{y,l}, \hat{s}^z_l], \tag{9}$$

where $H_{y,l}$ contains the terms in Eq. (1) involving sites l and $l+y$, τ is the time. Since on-site terms of the Hamiltonian could not lead to quantities considered as "currents", then $[H_{y,l}, \hat{s}^z_l]$ should be replaced by $[H_{0,y,l}, \hat{s}^z_l]$,[34] and the following expressions for $\hat{j}^s_y$ are obtained:

$$\begin{aligned}\hat{j}^s_y &= \hat{j}^s_{hop,y} + \hat{j}^s_{SO,y},\\ \hat{j}^s_{hop,y} &= \frac{1}{2}(\hat{j}_{\uparrow,y} - \hat{j}_{\downarrow,y}),\\ \hat{j}^s_{SO,y} &= -\frac{\lambda}{2}\sum_l (c^\dagger_{l+y\downarrow}c_{l\uparrow} - c^\dagger_{l+y\uparrow}c_{l\downarrow} + H.c.)\end{aligned} \tag{10}$$

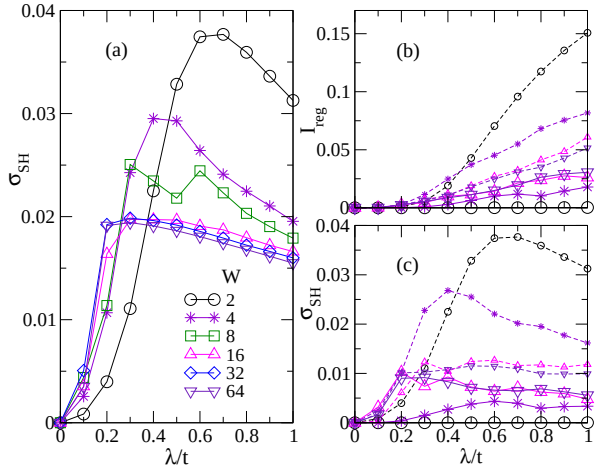

FIG. 4. (Color online) (a) spin-Hall conductivity, (b) inter- (dashed lines) and intra- (full lines) band contributions to I_{reg}, and (c) inter- and intra-band contributions to the spin-Hall conductivity, as a function of λ/t for various strip widths W indicated on the plot. Isolated, $J_{sd} = 0$, $L = 2000$ Rashba strips.

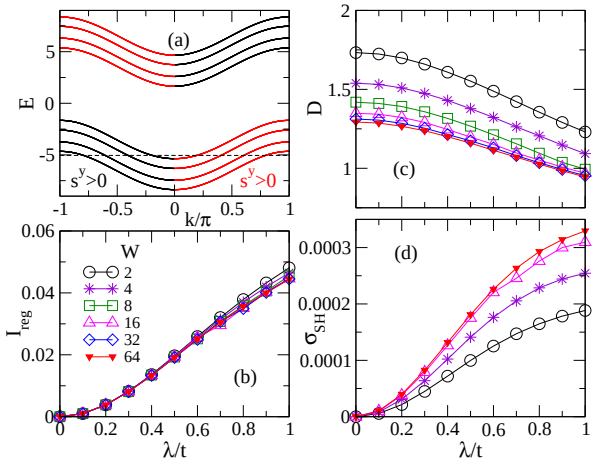

FIG. 5. (Color online) (a) Band structure for $W = 4$, $\lambda/t = 0.4$. (b) I_{reg}, (c) Drude weight, and (d) spin-Hall conductivity, as a function of λ/t for various strip widths W, for a fixed FM layer, $J_{sd} = 10$.

Clearly, from Eqs. (5) and (10), there will be in principle four independent contributions to σ_{sH} which are computed and studied separately.

A. Isolated Rashba strips

Let us start by examining isolated conducting Rashba strips ($J_{sd} = 0$). In Fig. 3(a), the single-particle bands, $E(k)$, where k is the momentum along x, is shown for $W = 4$, $\lambda/t = 0.4$. The RSOC splits each band into two bands with different sign of $s^y =< \hat{s}^y >_{sp}$. Note that for the strips here considered, as a difference with the case of the 2D system,[35] s^y is not a good quantum number. Also, due to the breaking of spatial rotational invariance, only the value of s^y, related to the momentum along the strip axis, is needed to label $\{k, E(k)\}$ points. Note also that on each of the bands, the sign of s^y may change.

In the following the expressions "interband transitions" or "intraband transitions" will refer to transitions between states with opposite or the same sign of s^y respectively. A typical interband transition contributing to the lowest peak in $\sigma(\omega)$ is shown in Fig. 3(a). The inter- and intraband contributions to I_{reg} and σ_{sH} will be discussed below.

Clearly, the behavior of $E(k)$ is metallic for all electron fillings, and for $n = 0.5$, the chemical potential is located close to a maximum of the density of states or van-Hove singularity. In Fig. 3(b), results for the integral of the regular part of the optical conductivity, I_{reg}, are shown as a function of λ/t for various strip widths indicated on the plot. The main result is that I_{reg} is due entirely to the SO currents defined in Eq. (5). The Drude weight D is shown in Fig. 3(c)). Both quantities present a non-monotonic behavior as a function of W, and cusps around $\lambda/t \approx 0.4 - 0.5$ can be noticed for $W = 2$ and 4, which is consistent with the behavior of the RHCs shown in Fig. 2(c),

In Fig. 4(a), the spin-Hall conductivity is shown for various strip widths as a function of λ/t. In this case, σ_{sH} turns out to be entirely due to the $< \hat{j}_{SO,x}\ \hat{j}^s_{hop,y} >$ (for short) contribution. σ_{SH} has a strong dependence with W, with a maximum shifting to lower vales of λ/t as W increases, although it seems that it is converging for $W = 64$. For the largest widths considered, $W = 32, 64$, the spin-Hall conductivity presents a flat region reminiscent of the constant value predicted in Ref. 23, although this prediction was obtained for the infinite 2D system with a parabolic dispersion. Notice also that with the normalization here adopted for the parameters t and λ, the energies are approximately independent of λ/t, while without this normalization, the energies depend approximately quadratically with λ/t. Hence, additional factors should have to be taken into account, due to the energies in the denominator of Eq. (8) . For these widest strips, the presence of a cusp separating two different regimes is clearly visible, and in this case, the cusp is not correlated with the peaks observed in the RHCs curves.

In Figs. 4(b,c) the inter- and intraband contributions to the I_{reg} and to σ_{sH} are shown. In both cases, it is remarkable that for $W = 2$ both quantities are purely of inter-band origin, and that as W increases the inter- and intraband processes tend to equally contribute to those quantities.

B. Coupled FM layer

Let us now consider the more interesting case of a fixed FM layer coupled to the conducting strip by a ferromag-

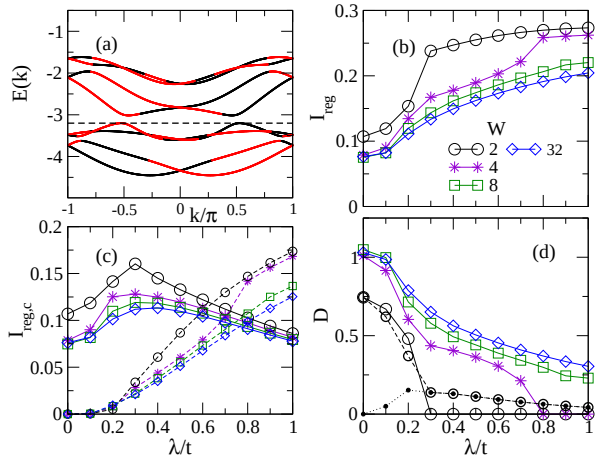

FIG. 6. (Color online) (a) Lower half of the band structure, $s^y > 0$ (black) or $s^y < 0$ (red), $W = 4$, $\lambda/t = 0.4$. (b) I_{reg}, and (c) contributions to I_{reg} from hopping (solid lines) and SO (dashed lines) currents, (d) Drude weight, as a function of λ/t, for coupled AFM layer, $J_{sd} = 5$. Results for $256 \times W$ strips with symbols for various W indicated on the plot. In (d), contributions to D from hopping (dashed line) and SO (dotted line) currents for $W = 2$ are also included.

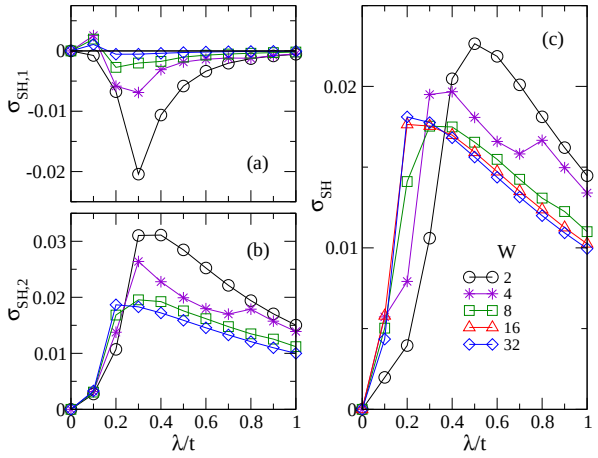

FIG. 7. (Color online) (a) $\sigma_{sH,1}$, and (b) $\sigma_{sH,2}$ contributions to the spin-Hall conductivity (see text), and (c) total spin-Hall conductivity, as a function of λ/t, for coupled AFM layer, $J_{sd} = 5$, with symbols for various W indicated on the plot.

netic exchange $J_{sd} = 10$. In Fig. 5(a), the dispersion relation for $W = 4$ and $\lambda/t = 0.4$ is depicted. $E(k)$ points have been labelled by the sign of s^y. The negative energy bands have also $s^z > 0$ and are separated from the positive energy bands with $s^z < 0$ due to the finite value $J_{sd} = 10$. The optical conductivity $\sigma(\omega)$ presents a single peak at $\omega \approx 10$ and it is originated in interband transitions, as can be inferred from the s^y character of the bands. In Fig. 5(b), I_{reg} is shown as a function of λ/t for various strip widths W. Again, this quantity is due entirely to the SO currents. and it is almost independent of W. The Drude weight, shown in Fig. 5(c), decreases as W increases due to a reduction of the kinetic energy along the longitudinal direction.

The spin-Hall conductivity, shown in Fig. 5(d), also presents a rather monotonic behavior as a function of λ/t. This monotonic behavior in both D and σ_{sH} is also consistent with the one observed for the RHCs in Fig. 2(a). The spin-Hall conductivity is also entirely due to the $< \hat{j}_{SO,x}\ \hat{j}^s_{hop,y} >$ contribution, and it almost entirely involve interband processes, except for marginal intraband contributions.

C. Coupled AFM layer

Let us finally examine the most important case which is the one of a Rashba conducting strip coupled to an AFM layer. Fig. 6(a) shows the lowest half energy bands of the $W = 4$ strip, $\lambda/t = 0.4$, where again $E(k)$ points have been labelled according to the sign of s^y. There is another set of energy bands symmetrically located with respect to $E = 0$. The two set of bands are separated in energy due to the finite $J_{sd} = 5$ value. A remarkable difference with respect to the two previous cases, is that the coupling to a AFM layer introduces small gaps whose sizes decreases with W and increases with J_{sd}. For $J_{sd} = 5$ the gap is present for $W \leq 8$, and disappears for $W \geq 16$. For $W \leq 8$ and $n = 0.5$, the Fermi level is just at the top of the energy branch below the gap, and hence close to a high density of states.

Fig. 6(b) shows I_{reg} for various strip widths W, and Fig. 6(d) the corresponding results for the Drude weight. For the smallest strip widths, $W = 2, 4$ there is a cusp at $\lambda/t \approx 0.3$, and $\lambda/t \approx 0.8$, that coincides with the value at which the respective Drude weights vanish. Notice that for widths $W > 2$, there is also a curvature change near $\lambda/t = 0.2$. It seems then that the decaying of the RHCs after their peak, shown in Fig. 7(b), may be correlated with the onset, for $W = 2$, or the proximity to a metal-insulator transition for $W > 2$. It is also interesting to note that the vanishing of the Drude weight for $W = 2,\ 4$ is due to equal and opposite contributions from spin-conserving and spin- flipping currents, as shown in Fig. 6(d) for $W = 2$.

As expected from the complex pattern of $E(k)$ points with positive and negative values of s^y, and as expected from the already discussed case of free Rashba strips ($J_{sd} = 0$), I_{reg} will have contributions from both inter- and intraband processes. More interesting, and perhaps more physically appealing, I_{reg} has now contributions from both the SO (spin-flipping) and the hopping (spin-conserving) currents, as shown in Fig. 6(b). As expected, the contribution from $\hat{j}_{hop,x}$ ($\hat{j}_{SO,x}$) dominates at small (large) λ/t, Contributions from the mixed term are marginal.

For the same reasons mentioned above, the spin-Hall conductivity will also have contributions from both inter- and intraband processes. However, what may be more interesting, is the fact that σ_{sH} has contributions from

both $< \hat{j}_{hop,x}\ \hat{j}^s_{hop,y} >$ and $< \hat{j}_{SO,x}\ \hat{j}^s_{hop,y} >$ terms. Contributions from the former lead to the term $\sigma_{sH,1}$, while contributions from the latter, to the term $\sigma_{sH,2}$. Results for $\sigma_{sH,1}$ and $\sigma_{sH,2}$ are shown in Figs. 7(a,b), respectively. The first conclusion is that both contributions have opposite signs, except for $\lambda/t \leq 1$, where both contributions are negative. It is also apparent that $\sigma_{sH,1}$ is suppressed faster with W. The total σ_{sH}, shown in Fig. 7(c) is hence dominated by the $< \hat{j}_{SO,x}\ \hat{j}^s_{hop,y} >$ terms. The discontinuous behavior above discussed is also noticeable in Figs. 7(a,b), where a clear change of behavior can be seen in $0.2 \leq \lambda/t \leq 0.3$, that is coincidentally with the peak in the RHCs shown in Fig. 2(b).

The resulting behavior of σ_{sH}, shown in Fig. 7(c) is strikingly different to the one for FM coupled layers. While for the FM layer, as shown in Fig. 5(c), σ_{sH} increases with both λ/t and W, for the AFM case, σ_{sH} reaches a maximum that decreases with W, and this maximum is located at a value of λ/t that also decreases with W. The overall behavior of σ_{sH} is also similar to the one already reported for isolated Rashba strips (Fig. 4(a)), including their magnitude.

Last but not least, it is remarkable that the maximum value of σ_{sH} in the AFM background is more than two orders of magnitude larger than the one for the FM case for the same W and at the same value of λ/t, and this difference is even larger for narrower strip widths.

V. INSTABILITIES OF THE AFM ORDER

Let us assume that the magnetic moments of the coupled layer can have an arbitrary orientation. As a first step, let us examine the case of a uniform orientation of the magnetic moments forming an angle θ with respect to the z-axis and an azimuthal angle φ with the x-axis, with the constraint that magnetic moments on nearest neighbor sites are opposed, that is, maintaining the AFM order. Of course, in the absence of a Rashba SO coupling, the system is independent of θ, φ. For any non-zero λ, the physical properties will depend on the global orientation of the magnetic moments. Actually, by minimizing the ground state energy of Hamiltonian (1), it turns out that the lowest energy state with uniform orientation of the magnetic moments corresponds to $\theta = \varphi = 0$, that is, pointing along the z-axis, for any value of J_{sd}. The value of J is irrelevant since for uniform orientation of magnetic moments it would contribute to a constant independent of λ.

Alternatively, the magnetic moment orientation may be fixed by the structure of the materials involved in a given device, so it is interesting to examine the dependence of transport properties with different orientations. In the following two different global orientations of the magnetic moments, $\theta = \pi/3$ and $\pi/2$, with $\varphi = 0$, will be analyzed. Resuming the comment after Eq. (9), notice that now due to the x-component of the magnetic moments, both $\hat{s}^z$ and the occupation number operators, n_σ, do not conmute with H_{int}. However, the resulting contributions from these conmutators are local, field-like operators, no current-like ones. Hence, in the following, the previous expressions for charge and spin currents, given by Eq. (5) and Eq. (10), respectively, will be used to compute the optical and spin-Hall conductivities.

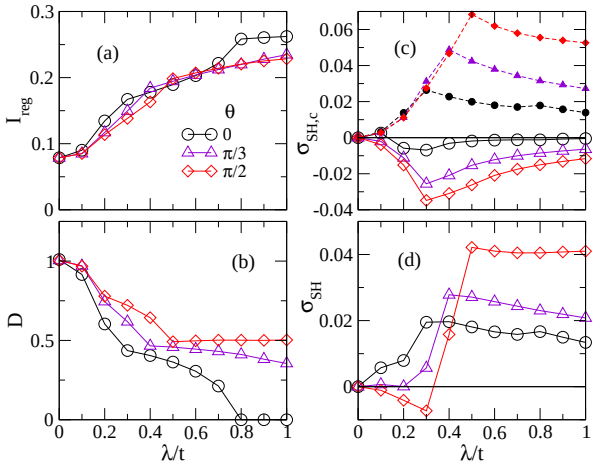

FIG. 8. (Color online) (a) Integral of the regular part of the optical conductivity, (b) Drude weight, (c) $\sigma_{sH,1}$ (full lines) and $\sigma_{sH,2}$ (dashed lines) contributions to the spin-Hall conductivity (see text), and (d) total spin-Hall conductivity, as a function of λ/t, for coupled AFM layer, $J_{sd} = 5$, $W = 4$, and various orientations of the order parameter with respect to the z-axis, given by the angle θ indicated on the figure. The azimuthal angle $\varphi = 0$.

Results for these two global orientations of the magnetic moments, for the $W = 4$ strip, $J_{sd} = 5$, are shown in Fig. 8, together with previous results for $\theta = \varphi = 0$ which are included for comparison. Fig. 8(a) shows that I_{reg} does not depend significantly on θ. On the other hand, the Drude weight systematically increases with θ, particularly for $\lambda/t > 0.5$, as shown in Fig. 8(b), and this behavior can be attributed to the closing of the gaps shown in Fig. 6(a). However, even for $\theta = \pi/2$, a change in the curvature can still be clearly observed. The total spin-Hall conductivity is shown in Fig. 8(d). At small values of the RSOC, σ_{sH} decreases with θ, while for larger values of the RSOC, it increases with θ. This behavior could be traced to the behavior of the two nonzero contributions to σ_{sH}, shown in Fig. 8(c). For small λ/t, the $\sigma_{sH,1}$ contribution, due to the $< \hat{j}_{hop,x}\ \hat{j}^s_{hop,y} >$ terms, grows rapidly with θ, while $\sigma_{sH,2}$, due to the $< \hat{j}_{SO,x}\ \hat{j}^s_{hop,y} >$ terms, is virtually independent of θ. For large λ/t, $\sigma_{sH,2}$ grows in absolute value more rapidly than $\sigma_{sH,1}$, thus leading to the observed change in the behavior of the total σ_{sH}.

If individual magnetic moments are allowed to rotate in order to minimize the ground state energy of Hamiltonian (1), it is found that the AFM order is unstable towards an AFM spiral, for $J \lessapprox 0.5$. In this AFM spiral or double-spiral, the orientation of the magnetic moments in one

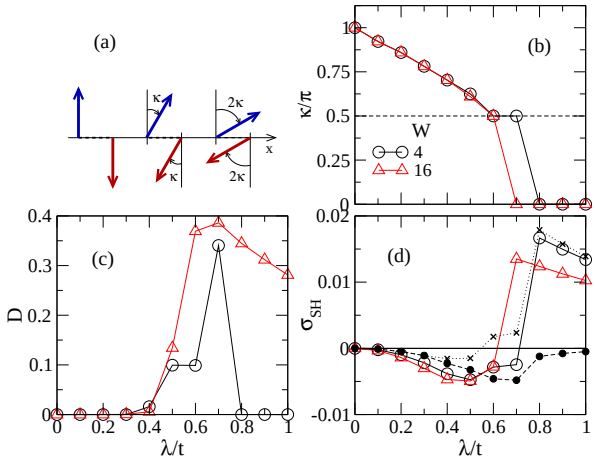

FIG. 9. (Color online) (a) Sketch of the AFM double-spiral along a chain. (b) Optimal pitch of the double-spiral, (c) Drude weight, and (d) total spin-Hall conductivity, as a function of λ/t, for coupled AFM double-spiral layer, $J_{sd} = 5$, $W = 4,\ 16$. In (d), $\sigma_{sH,1}$ (full circles) and $\sigma_{sH,2}$ (crosses) contributions for $W = 4$ have been added.

sublattice is given by $\theta = \kappa x$, and the magnetic moments on the other sublattice have the opposite directions thus keeping locally the AFM order, as illustrated in Fig. 9(a). This magnetic ordering of the coupled layer results from the interplay between the kinetic and magnetic energies of the Hamiltonian. In Fig. 9(b), the optimal pitch of the spiral, κ, is shown as a function of λ/t. For $\lambda = 0$, $\kappa = \pi$, corresponding to an order $\uparrow, \downarrow, \downarrow, \uparrow, \uparrow, \downarrow, \ldots$ along the longitudinal direction. As λ/t increases, κ decreases until it reaches the value $\pi/2$, and then there is a first-order transition to the AFM order ($\kappa = 0$). This behavior is mildly dependent on W and J_{sd}. In the region where κ is finite, particularly for $\lambda/t \leq 0.4$, the Drude weight (Fig. 9(c)) vanishes, and starts to grow as the transition to the AFM order approaches. This is a strikingly different behavior to the one observed in the AFM order, as shown in Fig. 7(b). This behavior is replicated by the spin-Hall conductivity, shown in Fig. 9(d), which is very small and negative for small λ/t, and then starts to grow, in absolute value, as the transition to the AFM order is approached. Beyond this transition point, σ_{sH} changes sign, taking the values already shown in Fig. 7(d). Notice that in the double-spiral region ($\kappa > 0$), the small value of σ_{sH} is not the result of the cancelation between the two contributions, $\sigma_{sH,1}$ and $\sigma_{sH,2}$, but from the sum of two small values of them.

For $J_{sd} = 5$ or smaller, the AFM order is also unstable towards an order that is staggered along the y-direction and spiral along the x-direction, with $\theta = \kappa x$, κ varying linearly between 0 for $\lambda/t = 0$, and $\pi/2$ for $\lambda/t \approx 0.8$. This instability of the AFM order, driven by the conduction electrons, also disappears for $J \gtrapprox 0.5$.

The FM order for $J_{sd} > 5$ is also unstable towards an order that is uniform along the transversal direction and spiral along the longitudinal direction again with a pitch κ varying linearly between 0 and $\pi/2$ as in the previously mentioned staggered spiral order, which is stable for $J_{sd} < 5$. A systematic study of these spiral orders will be presented in a forthcoming study.[30]

VI. CONCLUSIONS

In this work, the effects of finite strip widths on transport properties of Rashba conducting strips coupled to layers with various magnetic orders have been studied numerically at zero temperature.

In the first place, it was found that for the uncoupled Rashba strip (or coupled to a non-magnetic layer), the Drude weight slightly decreases with the Rashba SO coupling, and has a weak dependence with W. For a Rashba strip coupled to a FM layer, the Drude weight also slightly decreases with λ/t but it is strongly reduced by increasing the strip width. In both cases, the Rashba SO coupling reduces the Drude weight through processes involving solely the SO or spin-flipping currents. In addition, in the case of the FM coupling, the processes contributing to the optical conductivity are of interband origin, that is, connecting states with opposite signs of s^y. In contrast, for the uncoupled Rashba strips, these processes are completely of interband nature for the narrowest strip with $W = 2$, but the contribution from intraband transitions starts to grow with increasing W until it becomes approximately equal to the one of interband transitions, in the whole range of λ/t examined.

For the AFM coupled layer, due to the opening of gaps in the single-particle spectrum, the Drude weight has a more complex behavior. For all strip widths and Rashba SO couplings considered, its value is in general much smaller than for the other two cases studied, and it is much strongly supressed by λ/t. This suppression is due both to processes involving spin-conserving and spin-flipping currents. For the marrowest strips, $W = 2,\ 4$, D even vanishes at some finite value of λ/t. Certainly, this different behavior with respect to the other two cases, which are metallic, indicates the proximity to an insulating behavior in the AFM case.

Of course, the most relevant results for spintronic applications are those concerning the spin-Hall conductivity. In this sense, the main result is that σ_{sH} in the coupled AFM system is nearly two orders of magnitude larger than the one in the coupled FM system for virtually all values of W and λ/t. It would be tempting to relate this result with the recent finding of Néel-spin orbit torques driving domain walls at velocities two orders of magnitude greater than the ones in ferromagnets,[18,19] but this feature belongs to off-equilibrium regimes.

It is also important to emphasize that, for strips coupled to an AFM layer, a larger value of σ_{sH} is achieved for narrow (wide) strips at large (small) values of the Rashba SO coupling. The crossover between both regimes occurs at a value of λ/t that approximately coincides with the value at which a peak appears on the edge helical cur-

rents. Actually, the behavior of σ_{sH} with W and λ/t is quite similar to the one obtained for uncoupled Rashba strips. However, in the uncoupled case, σ_{sH} is entirely due to processes involving charge SO currents along x and spin hopping currents along y, while in the AFM case, there are also contributions from processes involving spin hopping currents along y, although these contributions have opposite sign to the former ones, except for $\lambda/t < 0.1$.

The orientation of the magnetic moments for the AFM coupled layer[19] has also been examined. It is interesting to note that for $W = 4$, σ_{sH} is largest at small λ/t when the magnetic moments are oriented along the z-direction, while for magnetic moments oriented along the x-axis, which is the case studied in Ref. 15, σ_{sH} is largest at large λ/t.

Finally, in systems where the conducting-magnetic layers exchange J_{sd} is due to a Hund coupling between conducting and localized orbitals of a transition metal oxide, which may be the case of devices involving $SrTiO_3$ interfaces, the ordering of the magnetic moments is determined by the dynamics of the competing degrees of freedom. In these systems, the AFM order become unstable at small and intermediate values of λ/t with respect to a double spiral order, where both the Drude weight and σ_{sH} essentially vanish for all W.

ACKNOWLEDGMENTS

Useful discussions with C. Gazza, I. Hamad, and G. Meza, are gratefully acknowledged. The author is partially supported by the Consejo Nacional de Investigaciones Científicas y Técnicas (CONICET) of Argentina through grant PIP No. 11220120100389CO.

[1] S. A. Wolf, D. D. Awschalom, R. A. Buhrman, J. M. Daughton, S. von Molnar, M. L. Roukes, A. Y. Chtchelkanova, D. M. Treger, Science **294**, 1488 (2001).

[2] G.A. Prinz, Science **282**, 1660 (1998).

[3] I. Zutic, J. Fabian, and S. Das Sarma, Rev. Mod. Phys. **76**, 323, (2004).

[4] D. Awschalom, Physics **2**, 50 (2009).

[5] E. I. Rashba, Sov. Phys. Solid State **2**, 1109 (1960); Y. A. Bychkov and E. I. Rashba, JETP Lett. **39**, 78 (1984).

[6] R. Winkler, *Spin-Orbit Coupling Effects in Two-Dimensional Electron and Hole Systems* (Springer, New York, 2003).

[7] J. Sinova, S. O. Valenzuela, J. Wunderlich, C.H. Back, and T. Jungwirth, Rev. Mod. Phys. **87**, 1213 (2015).

[8] A. Hoffmann, IEEE Transactions on Magnetics **49**, 5172 (2013).

[9] A. Manchon and S. Zhang, Phys. Rev. B **78**, 212405 (2008).

[10] A. Manchon and S. Zhang, Phys. Rev. B **79**, 094422 (2009).

[11] X. Wang and A. Manchon, Phys. Rev. Lett. **108**, 117201 (2012).

[12] I. M. Miron, G. Gaudin, S. Auffret, B. Rodmacq, A. Schuhl, S. Pizzini, J. Vogel and P. Gambardella, Nature Mater. **9**, 230 (2010).

[13] D. A. Pesin and A. H. Mac Donald, Phys. Rev. B **86**, 014416 (2012).

[14] A. S. Núñez, R. A. Duine, P. Haney, and A. H. MacDonald, Phys. Rev. B **73**, 214426 (2006).

[15] J. Zelezny, H. Gao, K. Vyborny, J. Zemen, J. Masek, A. Manchon, J. Wunderlich, J. Sinova, and T. Jungwirth, Phys. Rev. Lett. **113**, 157201 (2014).

[16] P. E. Roy, R. M. Otxoa, and J. Wunderlich, Phys. Rev. B **94**, 014439 (2016).

[17] P. Wadley, B. Howells, J. Zelezny, C. Andrews, V. Hills, R. P. Campion, V. Novak, F. Freimuth, Y. Mokrousov, A. W. Rushforth, K. W. Edmonds, B. L. Gallagher, and T. Jungwirth, Science **351**, 157201 (2016).

[18] O. Gomonay, T. Jungwirth, and J. Sinova, Phys. Rev. Lett. **117**, 017202 (2016).

[19] J. Zelezny, H. Gao, A. Manchon, F. Freimuth, Y. Mokrousov, J. Zemen, J. Masek, J. Sinova, and T. Jungwirth, arXiv:11604.07590.

[20] Y. Kato, R. C. Myers, A. C. Gossard, and D. D. Awschalom, Science **306**, 1910 (2004).

[21] T. Jungwirth, J. Wunderlich, and K. Olejník, Nature Mater. **11**, 382 (2012).

[22] J. A. Riera, Phys. Rev. B **88**, 045102 (2013).

[23] J. Sinova, D. Culcer, Q. Niu, N. A. Sinitsyn, T. Jungwirth, and A. H. MacDonald, Phys. Rev. Lett. **92**, 126603 (2004).

[24] E. I Rashba, Phys. Rev. B **70**, 201309 (2004).

[25] P. L. Krotkov and S. Das Sarma, Phys. Rev. B **73**, 195307 (2006).

[26] H. Y. Hwang, Y. Iwasa, M. Kawasaki, B. Keimer, N. Nagaosa, and Y. Tokura, Nature Mater. **11**, 103 (2012).

[27] S. Banerjee, O. Erten and M. Randeria, Nature Phys. **9**, 626 (2013).

[28] I. J. Hamad, C. J. Gazza, and J. A. Riera, Phys. Rev. B **93**, 205113 (2016).

[29] G. A. Meza and J. A. Riera, Phys. Rev. B **90**, 085107 (2014).

[30] G. A. Meza and J. A. Riera, unpublished.

[31] N. Bovenzi, F. Finocchiaro, N. Scopigno, D. Bucheli, S. Caprara, G. Seibold and M. Grilli, J. Supercond. Nov. Magn. **28**, 1273 (2015).

[32] S. Caprara, F. Peronaci, and M. Grilli, Phys. Rev. Lett. **109**, 196401 (2012).

[33] R. M. Fye, M. J. Martins, D. J. Scalapino, J. Wagner, and W. Hanke Phys. Rev. B **44**, 6909 (1991).

[34] In addition, $[H_{int,y,l}, \hat{s}_l^z] = 0$, if the direction of the magnetic moments is along the z-direction.

[35] S. D. Ganichev and L. E. and Golub, Phys. Status Solidi B **251** 1801 (2014).